with and without L_k) is shown in Figure 5. With this set of measurement data, it is also observed that without L_k there will be large discrepancy between the equivalent circuit model fitted and the measured results, which further confirms that the kinetic inductance plays an important role in the equivalent circuit model of the intrinsic SWCNT.

The RF conductance (calculated as the reciprocal of the summation of R_{cnt}, R_{c1}, and R_{c2}) for both measurements as a function of the gate bias voltage is plotted in Figure 6. Compared to the DC characterization of the device, it is seen that the fitted RF conductance at zero gate bias from the 1st measurement roughly agrees with the DC conductance, which is about 10 μS. As for the 2nd measurement, the RF conductance at zero gate bias is about 33 μS, which is higher than the DC conductance measured earlier.

3 | CONCLUSION

In conclusion, tapered CPW transmission-line test fixture with reduced parasitic effect and mismatch has been designed to measure the intrinsic microwave properties of suspended and pristine individual SWCNTs. Equivalent circuit model of SWCNT has been utilized to fit the de-embedded measured data. Kinetic inductance of the intrinsic SWCNT is successfully measured. Two sets of microwave measurements performed between about a year interval are compared. Different gate dependences are observed for these two measurements and the difference is attributed to the fact that the CNT-FET device's exposure to oxygen. The equivalent circuit model of individual SWCNT will be useful for future high-frequency nanocircuit applications.

REFERENCES

[1] Iijima S. Helical microtubules of graphitic carbon. *Nature.* 1991; 354:56–58.

[2] Cao Y, Brady GJ, Gui H, Rutherglen C, Arnold MS, Zhou C. Radio frequency transistors using aligned semiconducting carbon nanotubes with current-gain cutoff frequency and maximum oscillation frequency simultaneously greater than 70 GHz. *ACS Nano.* 2016;10:6782–6790.

[3] Hanson GW. Fundamental transmitting properties of carbon nanotube antennas. *IEEE Trans Antennas Propag.* 2005;53: 3426–3435. Nov.

[4] Maksimenkoa SA, Slepvana GY, Nemilentsau AM, Shubaa MV. Carbon nanotube antenna: Far-field, near-field and thermal-noise properties. *Phys E.* 2008;40:2360–2364.

[5] Wang L, Zhou R, Xin H. Microwave (8–50 GHz) characterization of multiwalled carbon nanotube papers using rectangular waveguides. *IEEE Trans Microw Theory Tech.* 2008;56(2):499–506.

[6] Wu Z, Wang L, Peng Y, Young A, Seraphin S, Xin H. Terahertz characterization of multi-walled carbon nanotube films. *J Appl Phys.* 2008;103(9):094324–1–094324–6.

[7] Tselev A, Woodson M, Qian C, Liu J. Microwave impedance spectroscopy of dense carbon nanotube bundles. *Nano Lett.* 2008;8(1):152–156.

[8] ZhangHuo MX, Chan PC, Liang HQ, Tang ZK. Radio-frequency transmission properties of carbon nanotubes in a field-effect transistor configuration. *IEEE Electron Device Lett.* 2006; 27(8):668–670.

[9] Tuo M, Wang L, Amer MR, Yu X, Cronin SB, Xin H. Microwave properties of suspended single-walled carbon nanotubes with a field-effect transistor configuration. *IEEE Int Microw Symp.* Baltimore, MD, 2011.

[10] Plombon JJ, O'brien KP, Gstrein F, Dubin VM, Jiao Y. High-frequency electrical properties of individual and bundled carbon nanotubes. *Appl Phys Lett.* 2007;90:063106–1–063106–3.

[11] Rutherglen C, Burke P. Nanoelectromagnetics: circuit and electromagnetic properties of carbon nanotubes. *Small.* 2009;5: 884–906.

[12] Collins PG, Bradley K, Ishigami M, Zettl A. Extreme oxygen sensitivity of electronic properties of carbon nanotubes. *Science.* 2000;287:1801–1804.

[13] Amer MR, Bushmaker AW, Cronin SB. Anomalous kink behavior in the current-voltage characteristics of suspended carbon nanotubes. *Nano Res.* 2012;5:172–180.

Compact leaky wave antenna using ferroelectric materials

H. M. Jeon | Z. Ji | Y. Zhuang

Department of Electrical Engineering, Wright State University, Dayton, Ohio

Correspondence
Y. Zhuang, Wright State University, Electrical Engineering, 3640 Colonel Glenn Hwy, Dayton, Ohio, United States 45435.
Email: yan.zhuang@wright.edu

Abstract

In this work, we present a leaky wave antenna with an enhanced angular scan rate (ASR) using high permittivity materials. The proto-type leaky wave antenna consists of a

copper-made rectangular waveguide filled with lead zirconate titanate (PZT). The effective permittivity of the rectangular waveguide is tuned by varying the thickness of the PZT. The antenna showed an ASR of 265°/GHz between 2.4 GHz and 2.6 GHz as the effective permittivity is 337, and an ASR 636°/GHz between 2.12 GHz and 2.23 GHz as the effective permittivity is increased to 813.

KEYWORDS

antenna, ferroelectric, leaky wave, RF

1 | INTRODUCTION

Leaky wave antenna (LWA) attracts tremendous attention for capable of electrical steering of the radiation beam.[1,2] Traditional air-core LWAs suffer from the long propagation wavelength, and thus large volume. In addition, a broad frequency tuning band (FTB) is required for air-core LWAs to achieve a wide angle scan. LWA with a 3 GHz (15–18 GHz) FTB has been reported to achieve of 30 degree scanning angle (SA).[1] A microstrip LWA showed a 143 degree SA with a 4.4 GHz FTB.[3] Generally a greater SA demands for a wider FTB. Unfortunately, such broad FTB impedes the application of LWAs in personal communications, which requires the system be capable of operation at a fixed frequency or in a narrow frequency band. For example, according to the international, regional and national regulation, the unlicensed industrial scientific, and medical (ISM) frequency bands are scattered between 7.78 KHz and 245 GHz. The bandwidth of the ISM is less than 0.25 GHz as frequency below 24.125 GHz, and less than 2.0 GHz as frequency approach to 245 GHz. This imposes a formidable challenge on LWA to achieve large SA with a narrow FTB for example less than 0.25 GHz for ISM applications below 24.125 GHz.

Continuous efforts have been done to develop so-called fixed frequency LWAs, i.e. the radiation beam scanned at a fixed frequency.[4–6] This is achieved by modifying the propagation constant of the electromagnetic wave traveled in the LWAs while remains the frequency unchanged. The fixed frequency LWAs have been demonstrated by a few groups by loading adjustable lumped capacitors,[7] voltage controlled varactors,[8] and transmission lines with varied loads and spacing.[9] However, the SA achieved at fixed frequency is rather small, which is less than 30° in refs. [4–10]. The extra loadings also increase the complexity of circuit design and the cost in circuit fabrication.

An alternative to overcome the challenge is to develop LWAs with an enhanced angular scan rate (ASR), the ratio between SA and FTB. LWA using dielectric materials has been reported to have higher ASR.[11–16] Compared with the air-filled LWA, insertion of Perspex ($\varepsilon_r = 2.55$) led to a factor 4.5 increase in ASR for a 40.0 cm long LWA operated between 8.1 and 9.6 GHz.[12] The angular scan range up to 60°GHz has been achieved, but the FTB is well above 0.25 GHz. Both theoretical studies[17,18] and experimental results[19,20] have been reported of LWA on ferroelectric substrates, but direct implementation of ferroelectric materials in LWAs to enhance its performance such as ASR is still missing.

In this work, we present a LWA with an enhanced ASR using ferroelectric materials due to the high relative permittivity (ε_r). Lead Zirconate Titanate (PZT, American Piezo Ceramics, Inc.) was used for its high relative permittivity $\varepsilon_r \sim 1900.0$. The effective permittivity ($\varepsilon_{r\text{-effe}}$) of the LWA is varied by changing the thickness of the PZT inserted in the LWA. By increasing in $\varepsilon_{r\text{-effe}}$, the LWA shows a more than 60 times increase in ASR, a lower operating frequency, and a narrower FTB. Numerical simulations have been carried out using Finite Element Method (FEM), which are in very good agreement with the experiments.

2 | EXPERIMENTS

The basic LWA structure consists of a copper rectangular waveguide with 13 slots array cut into its sidewall (Figure 1). The slot width (SW), length (SL), and distance (SD) are 1.0 mm, 6.0 mm, and 7.0 mm, respectively. The width, length, and height of the waveguide are WW = 8.0 mm, LW = 96.0 mm, and HW = 1.7 mm, respectively. Multiple pieces of PZT plate (American Piezo Ceramics, Inc.) were inserted in the waveguide to increase the $\varepsilon_{r\text{-effe}}$. Since the propagation wavelength at the operating frequency $\lambda \gg h_1$, and h_2 which are the thickness of printed circuit board (PCB) and PZT plates respectively, the $\varepsilon_{r\text{-effe}}$ can be calculated by averaging of the permittivity of the entire multilayer based on effective medium theory[21]:
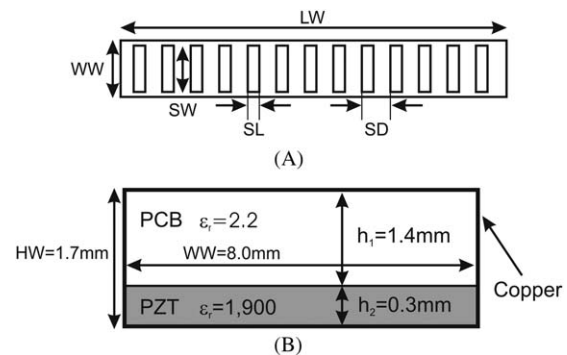

(A)

(B)

FIGURE 1 (A) Top view of a rectangular waveguide LWA; (B) Cross-sectional view of the rectangular waveguide LWA formed by a piece of PCB and three pieces of copper foils; the inserted PZT film has a thickness of 0.3 mm, and ε_r of ~1900
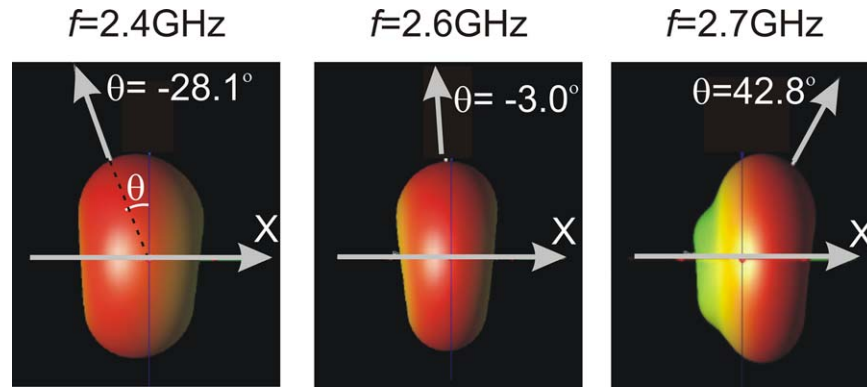
FIGURE 2 Simulated radiation patterns of a LWA having an effective dielectric constant $\varepsilon_r = 337$ at various frequencies from 2.4 GHz, to 2.6 GHz, and to 2.7 GHz. The structural parameters of the LWA are the same as shown in Figure 1. Arrows indicate the direction of the MRB (θ), and x parallel to the direction of the wave guide axis. [Color figure can be viewed at wileyonlinelibrary.com]

$$\varepsilon_{\text{r-effe}} = \frac{h_1 \times \varepsilon_{r\text{-PCB}} + h_2 \times \varepsilon_{r\text{-PZT}}}{h_1 + h_2} \quad (1)$$

Where $\varepsilon_{r\text{-PCB}}$ is the relative permittivity of PCB, and $\varepsilon_{r\text{-PZT}}$ is the relative permittivity of PZT plates.

During the measurements, the LWA was fed by an Agilent N9310A RF Signal Generator (9 kHz to 3 GHz) through a SMA connecter soldered on one side of the waveguide. A dipole antenna was used to detect the radiation signals and an Agilent N9320B RF Spectrum Analyzer (9 kHz to 3 GHz) was used to measure the radiation power. The distance between the LWA and dipole antenna was set to 50 cm. To improve spatial angular resolution, a slit was placed in front of the dipole antenna, achieving angular resolution ~20°.

3 | RESULTS AND DISCUSSIONS

The propagation wavelength (λ_{LWA}) of a traveling wave in LWA rectangular waveguide can be written to:

$$\lambda_{\text{LWA}} = \frac{2\pi}{\sqrt{\omega^2 \mu_0 \mu_r \varepsilon_0 \varepsilon_{\text{r-effe}} - \left(\left(\frac{m\pi}{\text{WW}}\right)^2 + \left(\frac{n\pi}{\text{HW}}\right)^2 \right)}} \quad (2)$$

where μ_0 and ε_0 are the magnetic permeability and electric permittivity of vacuum, μ_r and $\varepsilon_{\text{r-effe}}$ are the relative magnetic permeability and permittivity of the entire multilayer, respectively, m and n are integers. Since WW > HW, the lowest propagation mode in the LWA is TE_{10} ($m = 1$, $n = 0$). From Equation 2, insertion of high permittivity materials results in shortening of the propagation wavelength. This will increase the density of slots, thus the number of slots in a fixed length LWA. Because the radiation pattern from LWAs is essence the Fourier transform of the aperture distribution, the higher number of slots in an array reduces the radiation beam width, and suppress the radiation side lobes.[22] Meanwhile, the shorter wavelength can also lead to

a significant size reduction of LWA with similar radiation performance, i.e. the beam width and side lobes, by keeping the same number of the slots.

Simulations of antenna radiation pattern were performed using Electromagnetic Professional (EMPro-Keysight) based on FEM (Figure 2). The structural parameters of the LWA are given in Figure 1 with SW = 1.0 mm, SL = 6.0 mm, and SD = 7.0 mm. In the calculations, the effective permittivity of the materials filled in the LWA is $\varepsilon_r = 337$ to coincide to the $\varepsilon_{\text{r-effe}}$ of insertion of one piece of PZT film in the LWA (Figure 1): $\varepsilon_{\text{r-effe}} = 2.2 \times 1.4 + 1900.0 \times 0.3 / 1.4 + 0.3 = 337$. The arrows in Figure 2 indicate the direction of the main radiation beam (MRB). By varying the frequencies, the direction of MRB rotates clockwise from $\theta = -20°$ to $\theta = 35°$ as frequency increases from 2.4 GHz to 2.7 GHz, where the angle θ is measured from the broadside direction, i.e. perpendicular to the LWA's waveguide axis. The direction of MRB of LWA in general follows
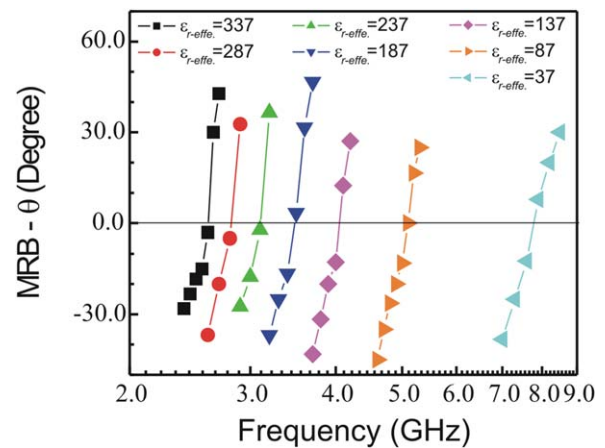

FIGURE 3 Simulated directions of MRB versus frequencies of LWAs filled with materials of having various $\varepsilon_{\text{r-effe}}$. [Color figure can be viewed at wileyonlinelibrary.com]
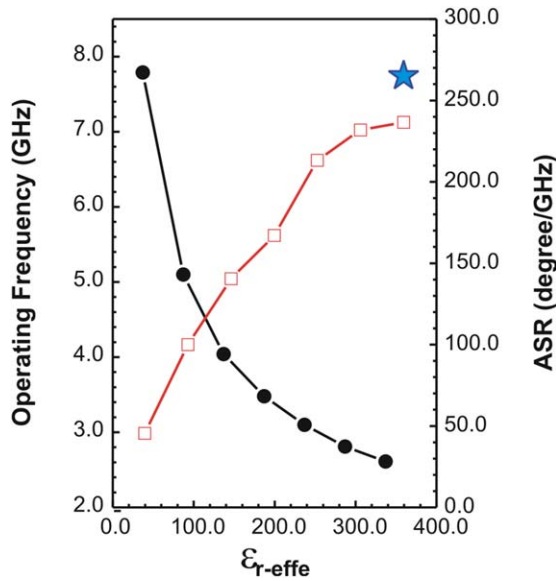
FIGURE 4 Simulated the directions of the MRB and the operating frequencies versus $\varepsilon_{\text{r-effe}}$. The blue start shows the measured result. [Color figure can be viewed at wileyonlinelibrary.com]

$$\sin \theta = \frac{\lambda_0}{\lambda_{\text{LWA}}} - \frac{\lambda_0}{\text{SD}} \cdot m \qquad (3)$$

Where λ_0 the wavelength in air, and m is an integer number. In Equation 3, the propagation wavelength $\lambda_{\text{LWA}} = \text{SD}$ when the direction of MRB perpendicular to the LWA's waveguide axis, i.e. $\theta = 0$. Thus in Figure 2, the propagation wavelength can be estimated to ~ 7.0 mm at 2.6 GHz, where
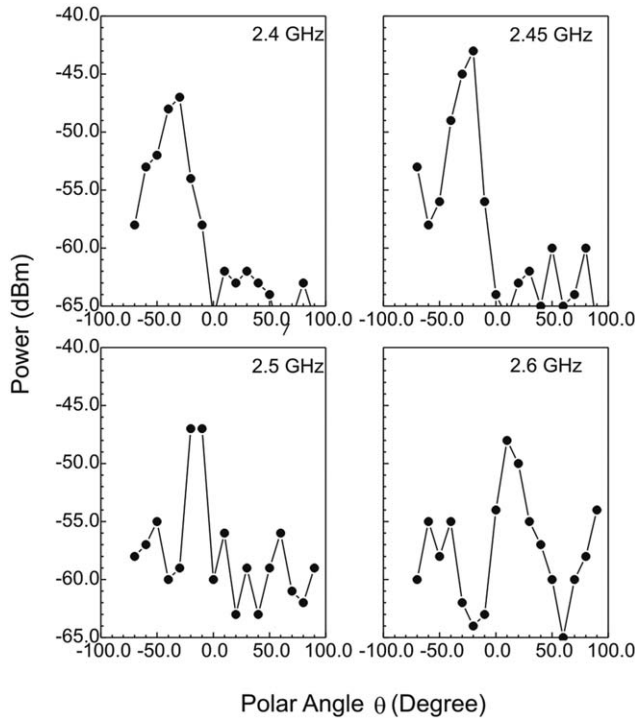

FIGURE 5 Measured radiation power of a LWA at different frequencies versus polar angle θ. The $\varepsilon_{\text{r-effe}}$ of the LWA is 337
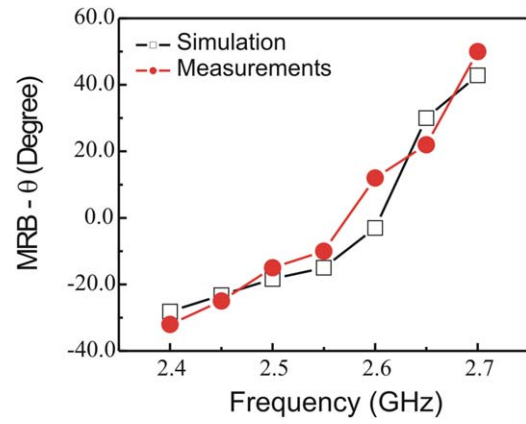

FIGURE 6 Comparison of measured and simulated directions of MRB of a LWA with $\varepsilon_{\text{r-effe}} = 337$. [Color figure can be viewed at wileyonlinelibrary.com]

$\theta = -3°$. The wavelength calculated in Equation 2 of TE_{10} ($m = 1$, $n = 0$) mode is ~ 6.8 mm by taking $\varepsilon_{\text{r-effe}} = 337$ which is in a good agreement with the FEM calculations. This validates the effective medium theory applied to estimate the effective permittivity of the LWA, and also indicates that the leaky waves were formed mainly from the TE_{10} mode wave in LWA. In this work, we optimized the structure (SD) of LWAs toward operating close to 2.4 GHz as an example, since this frequency band has been used ubiquitously in mobile communication and is an unlicensed in ISM. Similar method can be readily extended to other ISM frequency bands. It should be pointed out that the cut-off frequency of mode TE_{20} is 2.04 GHz, leading to excitation of mode TE_{20} between 2.4 GHz and 2.7 GHz in our simulations (Figure 2). This might reduce the radiation efficiency.

The directions of MRB versus frequency and $\varepsilon_{\text{r-effe}}$ were calculated and shown in Figure 3. Due to the nonlinear dependency between the direction of MRB and the frequency (Figure 3), the ASR is calculated by taking the mean slope of the curves, i.e. $\text{ASR} = \Delta\theta / \Delta f$, where $\Delta\theta$ is the maximum SA and Δf is corresponding tuning frequency. As $\varepsilon_{\text{r-effe}}$ increases, the ASR becomes larger (Figure 4). Meanwhile, the required frequency tuning range has also been significantly reduced. For example, frequency ranges of 0.25 GHz and 0.12GHz are required to scan $\pm 20°$ when the LWA waveguide is filled with materials of having $\varepsilon_{\text{r-effe}}$ of 137 and 337, respectively. In addition, due to the shortening of the propagation wavelength, larger $\varepsilon_{\text{r-effe}}$ also lowers the central operating frequency defined when $\theta = 0$ (Figure 4).

A LWA was fabricated by insertion one piece of PZT film in the waveguide with the $\varepsilon_{\text{r-effe}}$ estimated to be ~ 337. Its structural parameters are shown in Figure 1. The measured radiation power from the LWA shown in Figure 5 is well above the floor noise ~ -80 dBm. The maximum SA can reach up to 70° which is about 2.3-fold enhancement over the air core fixed frequency LWA.[4–10] As frequency

TABLE 1 Comparison of measured LWAs of having $\varepsilon_{r\text{-effe}}=337$ and $\varepsilon_{r\text{-effe}}=813$, with the LWA reported in refs. [1] and [12]

Permittivity (ε_r)	1 [1]	2.55 [12]	337	813
SA (°)	−65 to −35	10–50	−38 to 15	−30 to 40
Operating frequency (GHz)	15–18	8.1–9.1	2.4–2.6	2.12–2.23
ASR (°/GHz)	10	44	265	636

increases from 2.4 GHz to 2.6 GHz, the direction of MRB shifts from −38° to 15°, achieving to ASR 265°/GHz which is more than sixfold greater than the reported in ref. [5]. The measured ASR is slightly larger than the simulated results (Figure 4). It should be pointed out that the high ε_r materials also led to significantly lowering of the radiation power. The 3 dB beam width is about 20° to 30°, in a good agreement with the angular resolution of the measurement set-up. Figure 6 shows the comparison between the measurements and simulations by taking $\varepsilon_{r\text{-effe}}=337$, which are in a very good agreement.

As shown in Figures 3 and 4, higher $\varepsilon_{r\text{-effe}}$ leads to a larger ASR. To further enhance the ASR, a LWA with $\varepsilon_r=813$ was fabricated by insertion of multiple pieces of PZT in the rectangular waveguide. To have a similar operating frequency (∼2.4 GHz) as for $\varepsilon_r=337$, the SD is reduced to 4.8 mm. The propagation wavelength was estimated to ∼4.8 mm at 2.33 GHz, where θ=3°. The wavelength calculated in Equation 2 of TE_{10} ($m=1$, $n=0$) mode is ∼ 4.7 mm by taking $\varepsilon_{r\text{-effe}}=813$ in a good agreement with the FEM calculations. Table 1 lists the measurement results from two LWAs for $\varepsilon_r=337$ and $\varepsilon_r=813$. A factor of 2.4 enhancement of ASR has been obtained by increasing $\varepsilon_{r\text{-effe}}$ from 337 to 813.

Compared with air-core LWA[1] and dielectric-core with low permittivity,[11–16] the ASR has been improved from 10°/GHz, and 60°/GHz to 636°/GHz. In general, the unique features of ferroelectric materials based compact LWAs are (1) shorter length and (2) higher ASR. Moreover, since the permittivity of ferroelectric materials is controllable by applying external electric field, it provides an additional freedom to tune the radiation direction. Usually, high ε materials lower the operating frequency and the radiation power, thus a compromise design of radiation power, operating frequency and tuning sensitivity should be considered.

4 | CONCLUSIONS

In this work, by applying a high dielectric constant material onto the guiding structure, a low-cost, small size, light weight, and high sensitivity leaky-wave antenna is designed, implemented, and demonstrated. The proto-type leaky wave antennas showed close to 80 degree SA with FTB less than 0.11 GHz, which is fully met the demand for personal communications by

ISM requiring bandwidth less than 0.25 GHz as frequency below 24.125 GHz. The ASR has been achieved up to 265°/GHz for $\varepsilon_r=377$ and 636°/GHz for $\varepsilon_r=813$.

REFERENCES

[1] Hejase JA, Myers J, Kempel L, Chahal P. Design study of electronically steerable half-width microstrip leaky wave antennas. *IEEE Electron Components Technol Conf*. 2011:1348–1353.

[2] Jackson DR, Caloz C, Itoh T. Leaky-wave antennas. *Proc IEEE*. 2012;100:2194–2206.

[3] Li Y, Xue Q, Tan H-Z, Long Y. The half-width microstrip leaky wave antenna with the periodic short circuits. *IEEE Trans Antennas Propag*. 2011;59:3421–3423.

[4] Li Y, Long Y. Frequency-fixed beam-scanning microstrip leaky-wave antennas. *IEEE Soc Int Conf Antennas Propag*. 2003;2:1146–1149.

[5] Li Y, Long Y. Frequency-fixed beam-scanning microstrip leaky-wave antenna with multi-terminals. *Electron Lett*. 2006;42:10–11.

[6] Li Y, Xue Q, Yung EKN, Long Y. Dual-beam steering microstrip leaky wave antenna with fixed operating frequency. *IEEE Trans Antennas Propag*. 2008;56:248–252.

[7] Augustin G, Shynu SV, Aanandan CK, Mohanan P, Vasudevan K. A novel electronically scannable log-periodic leaky-wave antenna. *Microw Opt Technol Lett*. 2005;45:163–165.

[8] Guzman-Quiros R, Gomez-Tornero JL, Weily AR, Guo YJ. Electronically steerable 1-D Fabry-Perot leaky-wave antenna employing a tunable high impedance surface. *IEEE Trans Antennas Propag*. 2012;60:5046–5055.

[9] Liu J, Long Y. Analysis of a microstrip leaky-wave antenna loaded with shorted stubs. *IEEE Antennas Wireless Propag. Lett*. 2008;7:501–504.

[10] Karmokar DK, Esselle KP, Hay SG. Fixed-frequency beam steering of microstrip leaky-wave antennas using binary switches. *IEEE Trans Antennas Propag*. 2016;64:2146–2154.

[11] Bahl I, Gupta K. A leaky-wave antenna using an artificial dielectric medium. *IEEE Trans Antennas Propag*. 1974;22:119–122.

[12] Bahl I, Gupta K. Frequency scanning by leaky-wave antennas using artificial dielectrics. *IEEE Trans Antennas Propag*. 1975;23:584–589.

[13] Bahl I, Gupta K. Radiation from a dielectric-artificial dielectric slab. *IEEE Trans Antennas Propag.* 1976;24:73–76.

[14] Bahl I, Bhartia P. Leaky-wave antennas using artificial dielectrics at millimeter wave frequencies. *IEEE Trans Antennas Propag.* 1980;18:23–26.

[15] Guglielmi M, Boccalone G. A novel theory for dielectric-inset waveguide leaky-wave antennas. *IEEE Trans Antennas Propag.* 1991;39:497–504.

[16] Jackson DR, Oliner AA, Ip A. Leaky-wave propagation and radiation for a narrow-beam multiple-layer dielectric structure. *IEEE Trans Antennas Propag.* 1993;41:344–348.

[17] Yashchyshyn Y, Modelski J. The leaky-wave antenna with ferroelectric substrate. In Proc. 14th Int. Conf. Microwaves, Radar and Wireless Communications, MIKON – 2002. *Conf Proc.* 2002;1:218–221.

[18] Yashchyshyn Y, Modelski JW. Rigorous analysis and investigations of the scan antennas on a ferroelectric substrate. *IEEE Trans Microw Theory Tech.* 2005;53:427–438.

[19] Lovat G, Burghignoli P, Celozzi S. A tunable ferroelectric antenna for fixed frequency scanning applications, *IEEE Antennas Wireless Propag Lett.* 2006;5:353–356.

[20] Varadan VK, Varadan VV, Jose KA, Kelly JF. Electronically steerable leaky wave antenna using a tunable ferroelectric material. *Smart Mater Struct.* 1994;3:470–475.

[21] Nan C. Effective-medium theory of piezoelectric composites. *J Appl Phys.* 1994;76:1155–1163.

[22] Schwering FK, Peng ST. Design of dielectric grating antennas for millimeter wave applications. *IEEE Trans Microw Theory Tech.* 1983;31:199–209.

How to cite this article: Jeon HM, Ji Z, Zhuang Y. Compact leaky wave antenna using ferroelectric materials. *Microw Opt Technol Lett.* 2017;59:2614–2619. https://doi.org/10.1002/mop.30781

Compact tunable lowpass filter with sharp roll-off and low insertion loss

Ting Zhang[1] (ORCID) | **Zongqi Cai**[1] |
Yang Yang[2] | **Jingfu Bao**[1] |
Yiwen Wang[3]

[1] School of Electronic Engineering, University of Electronic Science and Technology of China, Chengdu 611731, China

[2] Global Big Data Technology Centre, University of Technology Sydney, Sydney, New South Wales 2007, Australia

[3] School of Microelectronics and Solid-State electronics, University of Electronic Science and Technology of China, Chengdu 611731, China

Correspondence
Ting Zhang, University of Electronic Science and Technology of China, School of Electronic Engineering, No. 2006, Xiyuan Ave., West Hi-Tech Zone, Chengdu, Sichuan, China 611731.
Email: tingzhang.uestc@hotmail.com

Abstract

A novel continuously tunable lowpass filter (LPF) with compact size, sharp roll-off and low insertion loss is presented in this paper. The filter employs two varactor diodes, a pair of open-ended coupled lines and a U-shape step impedance line (SIL) with an open-ended stub loaded at the center of the SIL to form a very compact layout. The odd- and even-mode analysis and equivalent circuit model are demonstrated for estimation of the transmission characteristics. Tuning the DC voltage applied on the varactor diodes, the varactor capacitance accordingly changes leading to a varying cutoff frequency f_c. The measured results show that the achieved 3-dB f_c tuning range is 60.6% (1.15–2.15 GHz). The measured insertion loss (IL) and roll-off rate are 0.2-0.4 dB and 50–73 dB/GHz, respectively. The overall size of the LPF is only $0.005\lambda_g^2$, which shows a competitive advantage comparing with the state-of-the-art work.

KEYWORDS

odd- and even-modes, roll-off, tunable lowpass filter, varactor diode

1 | INTRODUCTION

As one of the core components in wireless communication systems, lowpass filters (LPF) with sharp roll-off frequency response, low insertion loss and compact size play an important role in down-conversion link of the receivers.[1] Recently, the frequency-tunable LPF designs have been comprehensively studied using various technologies, such as defected ground structure (DGS)[2] and complementary split ring resonator-split ring resonator (CSRR-SRR).[3] It is noted that the tunable LPF is highly desired in the reconfigurable wireless communication systems. Huang et al. presented a coplanar waveguide (CPW) tunable lowpass filter with the tuning range of 49% and a size of $0.2 \times 0.318 \ \lambda_g^2$.[4] Ni and Hong proposed a continuously tunable microstrip LPF with a sharp roll-off,[5] however, it has a complicated tuning mechanism